Electronic Structure, Chemical Bonding, and Vibronic Coupling in Mn^{IV}/Mn^{III} Mixed Valent $Li_xMn_2O_4$ Spinels and Their Effect on the Dynamics of Intercalated Li: A Cluster Study Using DFT

M. Atanasov,*,† J.-L. Barras, L. Benco,‡ and C. Daul

Contribution from the Institute de Chimie Inorganique et Analytique, Universite de Fribourg, Perolles, CH-1700 Fribourg, Switzerland

Received February 12, 1999. Revised Manuscript Received November 8, 1999

Abstract: Density functional theory (DFT) calculations on the $Mn^{IV}{}_7O_{14}$ and Mn^{III}/Mn^{IV} mixed valent $Mn_7O_{14}{}^-$ clusters are reported and used to characterize the Mn−O bonding in $Li_xMn_2O_4$ spinel. A recipe is proposed of how to extract from calculations on clusters electronic hopping and charge transfer (CT) energy parameters and to use them in a semiempirical (Hubbard type) Hamitonian which simultaneously accounts for electronic correlation and translational symmetry. The first application of this approach to Mn_2O_4 shows that, in contrast with conventional band calculations, the 3d electrons of Mn are rather localized. Vibronic coupling due to the $2t_{2g}{}^3 2e_g{}^1$ configuration of Mn^{III} with the α_{1g} and the Jahn−Teller(JT) active ϵ_g modes is analyzed using DFT calculations of the mixed valent $Mn_7O_{14}{}^-$ cluster and is found to lead to a lengthening of the Mn−O bond and to tetragonally elongated octahedra accompanied by an appreciable stabilization energy(−0.445 eV). Vibronic coupling and electron hopping energies obtained from the DFT calculation are used to set up a simple model of small polaron for the Mn^{III}/Mn^{IV} spinels. The calculated energy barrier of electron transfer (0.34 eV, static JT-effect, d_{z^2} ground state) agrees well with the one deduced from polaronic conductivity data on $LiMn_2O_4$ (0.4 eV). In the case of an energetic equivalency of the d_{z^2} and $d_{x^2-y^2}$ orbitals (such as $Li_xMn_2O_4$, $x < 1$, dynamic JT-effect), this model provides the possibility for electron transfer with a very low activation energy. The electronic transfer from Mn^{III} to Mn^{IV} in $Li_xMn_2O_4$ ($0 < x \ll 1$) is predicted to be fast and thus expected to assist the diffusion of Li^+ through the interstitial spinel framework. The interaction of Li^+ with the electrochemically active $2e_g(Mn^{III})$ electron does screen Li^+ from large variation of the Madelung potential along its path from the octahedral 16c to the tetrahedral 8a site and thus lowers the potential barrier for its diffusion through the spinel lattice.

I. Introduction

In this paper we discuss the electronic structure and vibronic coupling in the Mn^{IV}/Mn^{III} mixed valent $Li_xMn_2O_4$ spinel in the light of DFT calculations on Mn−O clusters. We are seeking information about the chemical bonding and the energetics for electronic and ionic dynamics in $Li_xMn_2O_4$.

There has been considerable interest in the $Li_xMn_2O_4$ ($0 \le x \le 1$) spinel and the related phases because of their peculiar applications in the fields of electrochemistry and catalysis.[1−7] In the $Li_xMn_2O_4$ ($0 \le x \le 1$) spinels, Li^+ enters the tetrahedral (8a) while Mn^{III}/Mn^{IV} occupies the octahedral (16d) sites in a cubic close packed (ccp) oxygen framework. It was discovered that one could convert the spinel structure $LiMn_2O_4$ to predominantly pure MnO_2 while maintaining the structure derived from the spinel, i.e., with nearly all the Li^+ removed from the tetrahedral sites and with manganese remaining on the octahedral sites in the ccp oxygen framework.[3] The reversible insertion and extraction of Li in the Mn_2O_4 spinel and a high energy density are the key properties for the application of $Li_xMn_2O_4$ as cathode material for rechargeable Li batteries.[8−9] An insertion/extraction reaction requires reduction/oxidation of the host matrix and mobility of the Li^+ ions within the host. Li intercalated Mn_2O_4 is therefore an ionic-electronic conductor. Good electronic conductivity in a mixed valence system (1) is only possible on energetically equivalent sites a prerequisite which is likely to be fulfilled only for crystallographic equivalency.

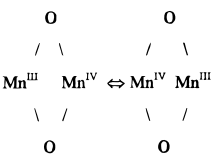

(1)

On the other hand, mobile d electrons may be itinerant or polaronic. If the time t for an electron to hop to a neighboring

* Address for corresponding author: Fachbereich Chemie der Philipps-Universität und Zentrum für Materialwissenschaften, Hans-Meerweinstr.1, D-35043 Marburg, Germany.

† Permanent address: Institute of General and Inorganic Chemistry, Bulgarian Academy of Sciences, Bl.11, 1113 Sofia, Bulgaria.

‡ Permanent address: Institute of Inorganic Chemistry, Slovak Academy of Sciences, Dubravska cesta 9, SK-84236 Bratislava, Slovakia.

(1) Barboux, P.; Tarascon, J. M.; Shokoohi, F. K. *J. Solid State Chem.* **1991**, *94*, 185.

(2) Tarascon, J. M.; McKinnon, W. R.; Coowar, F.; Bowmer, T. N.; Amatucci, G.; Guyomard, D. *J. Electrochem. Soc.* **1994**, *141*, 1421.

(3) Hunter, J. C. *J. Solid State Chem.* **1981**, *39*, 142.

(4) Thackeray, M. M.; Johnson, P. J.; de Picciotto, L. A.; Bruce, P. G.; Goodenough, J. B. *Mater. Res. Bull.* **1984**, *19*, 179.

(5) Pistoia, G.; Wang, G.; Wang, C. *Solid State Ionics* **1992**, *58*, 285.

(6) Martin, G. A.; Bates, A.; Ducarme, V.; Mirodatos, C. *Appl. Catal.* **1989**, *47*, 289.

(7) Masquelier, C.; Tabuchi, M.; Ado, K.; Kanno, R.; Kobayashi, Y.; Macki, Y.; Nakamura, O.; Goodenough, J. B. *J. Solid. State Chem.* **1996**, *123*, 255.

(8) Brandt, K. *Solid State Ionics* **1994**, *69*, 173.

(9) *Lithium Batteries Industrial Library*; Pistoia, G., Ed.; Elsevier: Amsterdam, 1994; Vol. 5.

10.1021/ja9904484 CCC: $19.00
Published on Web 04/29/2000

site is long compared to the period $T = \nu^{-1}$ of the optical mode that can trap it in a local potential well, then the electronic charge carriers are polaronic. A small polaron is a mobile electron (or hole) accommodated in a local, near-neighbor distorted surrounding. Its mobility is reduced by a factor $\exp(-\Delta E_a/kT)$, where ΔE_a is the activation energy needed to provide the energetic equivalency of the donor (Mn^{III}) and acceptor (Mn^{IV}) sites. On the other hand, the ionic conductivity, which is due to the mobility of Li^+ intercalated into the oxide host, depends on the variation of the Madelung potential for Li^+ along the path of its diffusion within the host and on the interaction between Li^+ and the charge compensating electron. In transition metal (TM) oxides these electrons occupy d orbitals of the TM ions.

The relation between the electronic and ionic properties of the $Li_xMn_2O_4$ ($0 \le x \le 1$) spinel system on its electronic structure remains an unsolved problem. This is because electronic structure calculations on this and other related systems such as the spinels (LiM_2O_4, M = Ti,Co) and the layered ($LiMO_2$, M = Ti, V, Mn, Co, Ni, Cu) structures have been confined to classical band theory which has a limited applicability for the systems under consideration. Although these calculations reproduce average battery voltages sometimes astonishingly well,[10−15] they describe less accurately the electronic correlation between the rather localized d electrons of the TM and overestimate charge fluctuation of the type (1). Both electronic correlation and fluctuations are of crucial importance in mixed-valent 3d compounds. In this respect, calculations on clusters [16] containing one or several TM ions are very promissing, because they allow us to control, in terms of orbital occupation numbers, different electronic configurations and to calculate changes in energy and geometry due to electronic charge transfer.

In this paper we report DFT calculations on the $Li_xMn_2O_4$ ($0 \le x \le 1$)spinel using Mn−O and Mn−O−Li clusters and use these results to characterize the extent of localization of the d electrons fixing Hubbard model parameters by a fit to data obtained from such constraint (cluster) DFT calculations. Geometrical relaxation which accompanies fluctuations of electronic charge is more pronounced in restricted clusters than in periodic solids. However, it is the wave function as obtained from calculation on clusters, rather than that resulting from a treatment of an extended periodic array, which being localized is more suitable for calculations of electron hopping and electron−phonon coupling parameters.

We focus first on $Mn^{IV}O_6$ clusters embedded in a surrounding of point charges and compare them with calculations on the smallest extended Mn_7O_{14} unit which is neutral and at the same time possess the correct Mn^{IV} site symmetry (D_{3d}). In section II we describe the choice of clusters for our calculations and the adopted computational scheme. In section III we present the results of the electronic structure and of the bonding in the single valent $Mn^{IV}{}_7O_{14}$ cluster (section III.1) and the vibronic (Jahn−Teller, JT) interactions in the $Mn^{III}O_6$ cluster (section III.2). The results of our cluster calculations yield Mn−Mn hoping integrals and energy barriers used to explore the electronic transport in mixed valent $Li_xMn_2O_4$ (section III.3). The procedure we describe enables to deduce for the first time the parameters of the polaronic model and to specify order of magnitudes of the different electronic mobilities in $Li_xMn_2O_4$ as a function of x ($0 \le x \le 1$). Comparison of these results with experimental conductivity provides a test for our theoretical calculations. Finally a qualitative discussion is given of how the electronic transport behavior in $Li_xMn_2O_4$ affect the dynamics of Li.

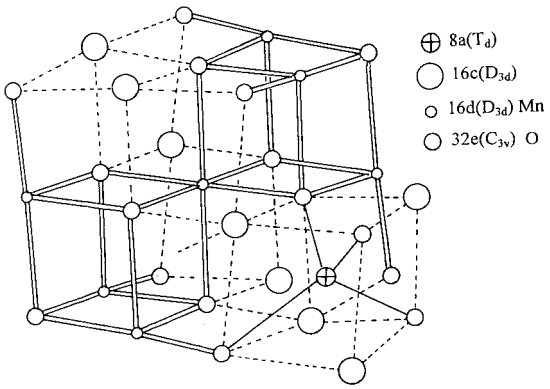

Figure 1. The basical structural motive of cubic spinel illustrating the relation of the structure of Mn_2O_4 to the rocksalt structure; the octahedral 16c,16d(Mn), pyramidal 32e(O), and the tetrahedral 8a sites are indicated.

II. Coordination Geometries of Mn in $Li_xMn_2O_4$ Spinels, Choice of Clusters, and the DFT Computational Scheme

The Mn_2O_4 spinel structure can be derived from the rocksalt structure in which one-half of the 32 octahedral sites (16d) are occupied by Mn atoms (Figure 1), the other half (16c sites, denoted by large circles in Figure 1) being empty. In addition, the 64 tetrahedral sites which are all empty in Mn_2O_4, become one-eight occupied (the circle of mean size in Figure 1) in the $LiMn_2O_4$ cubic spinel. The structure of spinels is completely described by the lattice parameter a and the oxygen position parameter x. Ideal octahedral geometry for the 16d site (D_{3d} symmetry) results if $x = {}^1/_4$. The following relations between the lattice parameters a and x, the M−O (R_{M-O}) and M−M (R_{M-M}) distances, the M−O-M bridging angle β and the angle between the C_3 axis and the M−O bond direction θ can be derived:

$$R_{M-M} = a/(2\sqrt{2}); \quad R_{M-O} = a(3x^2 - 2x + {}^3/_8)^{1/2}$$
$$\cos(\theta) = xa/(\sqrt{3}R_{M-O}); \quad \sin(\beta/2) = R_{M-M}/R_{M-O} \quad (2)$$

For $Li_{0.05}Mn_2O_4$, $a = 8.045$ Å and $x = 0.263$ have been reported,[17] implying MnO_6 polyhedra elongated along the C_3 axis (angle between C_3 and the Mn−O bond direction $\theta = 50.3°$, vs 54.74° in O_h). The Mn_7O_{14} cluster chosen in our calculations (Figure 2) consists of one Mn atom (Mn_1) in the center, surrounded by six O atoms, six second neighbor Mn_{2-7} atoms, and eight terminal O atoms coordinating these Mn atoms. This unit is still tractable quantum chemically at the DFT level, while preserving charge neutrality and the correct symmetry (D_{3d}) with respect to the central MnO_6 unit. For comparative purposes we have also performed calculations on the $Mn^{IV}O_6{}^{8-}$ cluster

(10) Ceder, G.; Chiang, Y.-M.; Sadoway, D. R.; Aydinol, M. K.; Jang, Y.-I.; Huang, B. *Nature* **1998**, *392*, 694.
(11) Aydinol, M. K.; Kohan, A. F.; Ceder, G.; Cho, K.; Joannopoulos, J. *Phys. Rev. B* **1997**, *56*, 1354.
(12) Benco, L.; Barras, J.-L.; Atanasov, M.; Daul, C.; Deiss, E. *Solid State Ionic* **1998**, *112*, 255.
(13) Benco, L.; Barras, J.-L.; Daul, C.; Deiss, E. *Inorg. Chem.* **1999**, *38*, 20.
(14) Wolverton, C.; Zunger, A. *J. Electrochem. Soc.* **1998**, *145*, 2424.
(15) Wolverton, C.; Zunger, A. *Phys. Rev. Lett.* **1998**, *81*, 606.
(16) Miura, K.; Yamada, A.; Tanaka, M. *Electrochim. Acta* **1996**, *41*, 249.
(17) Thackeray, M. M.; de Kock, A.; David, W. I. F. *Mater. Res. Bull.* **1993**, *28*, 1041.

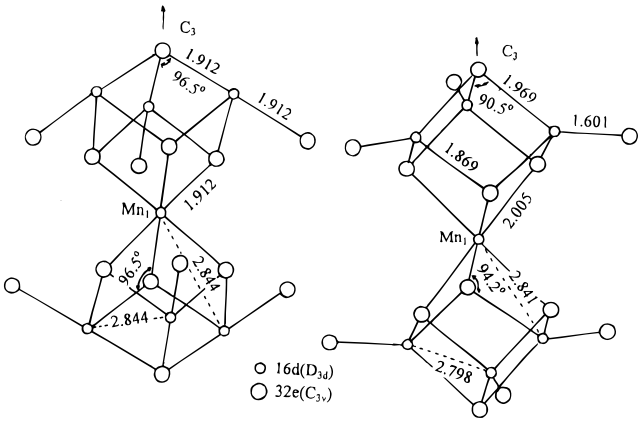

Figure 2. The geometries of the Mn_7O_{14} cluster extracted from the structure of (left) spinel and (right) DFT geometry optimized.

embedded in the electrostatic field of the remaining six Mn and eight O ions approximated here as +4 and −2 point charges.

All spin-restricted DFT calculations reported in this paper have been carried out with the Amsterdam density functional (ADF) program package (version 2.3).[18−22] The Vosko−Wilk−Nusair parametrization[23] of the electron gas data has been used for the exchange−correlation energy and potential. Density gradient corrections were included for the exchange[24] and for the correlation.[25] Triple-ζ Slater type orbitals (STOs), extended by by one polarization function (TZP) were used for Mn, O, and Li where core orbitals of Mn up to 2p were kept frozen.

III. Results and Discussion

III.1. Mn^{IV} −O Bonding and Electronic Structure of the $Mn^{IV}_7O_{14}$ Spinel Cluster. III.1.1. Orbital, Bonding Scheme, and Geometry of $Mn^{IV}O_6^{8-}$ and $Mn^{IV}_7O_{14}$. In octahedral ligand field, the 3d orbitals of Mn^{IV} split into two subsets of $t_{2g}(\pi)$ and $e_g(\sigma)$ orbitals. In addition a trigonal field (elongation along the C_3 axis) leads to the ordering of d orbitals and a $^4A_2(t_{2g}^3)$ ground state.

$$a_{1g}(t_{2g}) < e_g(t_{2g}) < e_g(e_g)$$

In Mn_7O_{14}, the set of d orbitals of six more Mn^{IV} ions yield $18t_{2g}(\pi)$ and $12e_g(\sigma)$ orbitals. They combine furthermore to yield a manifold of trigonally split cluster orbitals:

$$\begin{array}{ll} O_h & D_{3d} \\ t_{2g}(\pi): & 2a_{1g} + a_{2g} + a_{1u} + 2a_{2u} + 3e_g + 3e_u \\ e_g(\sigma): & a_{1g} + a_{2g} + a_{1u} + a_{2u} + 2e_g + 2e_u \end{array} \qquad (3)$$

For the ground state of the Mn_7O_{14} cluster, the orbitals originating from the oxygen $O^{2-}(2s,2p)$ and the metal $Mn^{IV}(t_{2g})$ are respectively occupied by eight and three electrons. Providing orbital occupations, consistent with this electronic distribution, a spin-restricted DFT geometry optimization was performed. The optimized cluster geometry as well as selected bond distances and angles are depicted in Figure 2 and compared

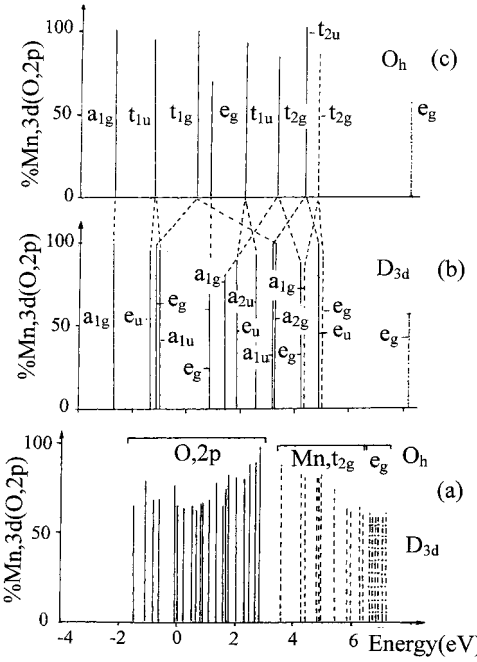

Figure 3. MO energies vs (solid lines) O,2p or (broken lines) Mn,3d orbital percentages of ligand and metal based orbitals, respectively, obtained from DFT calculations of the (a) optimized D_{3d} Mn_7O_{14} cluster and of MnO_6^{8-} embedded in a (b) surrounding of +4 and −2 point charges placed at the positions of the remaining Mn^{4+} and O^{2-} cluster atoms, respectively. The orbital level scheme for the MnO_6^{8-} with an ideal octahedral (O_h) geometry is also shown c. The position of the Mn−O nonbonding oxygen a_{2g} orbital is taken as energy reference in a. For the sake of comparison, the energy level scheme b is shifted such that the $a_{1g}(d_{z^2})$ orbitals of the central Mn in a and b coincide.

with the geometry of the corresponding fragment taken from X-ray structural analysis of $Li_{0.05}Mn_2O_4$.[17] The calculated Mn_1-O and Mn_1-Mn_{2-7} distances (2.005 and 2.840 Å) are respectively larger and close to the experimental data (1.912 and 2.844 Å[17]). The parameters $a = 8.036$ Å and $x = 0.251$ are calculated using eq 2. They are in reasonable agreement with experimental values ($a = 8.045$ Å and $x = 0.263$ [17]). Comparing the DFT optimized geometry with the experimental one, we note a considerable displacement of the terminal O atoms as compared to the crystal geometry. This is possibly an artifact due to an increased O−O repulsion in the cluster.

Calculated θ (54.5°) and β (90.2°) angles are correspondingly larger and smaller compared to the experimental ones (50.3° and 96.1°, respectively; see discussion below). The molecular orbital diagram of the MnO_6^{8-} cluster embedded in a surrounding of six $q_{Mn} = +4$ and eight $q_O = -2$ point charges is compared with that of Mn_7O_{14} in Figure 3b and a. Both sets of data pertain to the geometry (of atoms and point charges) of the DFT D_{3d} optimized Mn_7O_{14} cluster. For the sake of completness, the orbital level scheme for octahedral (O_h) geometry is also given (Figure 3c). Orbital energies and percentages of O,2p (solid lines) and Mn,3d (dashed, t_{2g} type and dotted, e_g type) show that these orbitals dominate, respectively, in the bonding, nonbonding, and antibonding combinations.

3d-Mn and 2p-O orbital contributions to the bonding and antibonding t_{2g},e_g orbitals (16%, 31% and 12%, 43%, respectively) reflect a predominantly ionic Mn−O bond, with a covalency which is larger for the $e_g(\sigma)$ orbitals, as compared to the $t_{2g}(\pi)$ ones. Surprisingly, the metal $4s(a_{1g})$ and $4p(t_{1u})$ contributions to the Mn−O bond are found negligibly small. The orbital reduction of the $O-2p(t_{1u})$ orbitals is mainly due

(18) Baerends, E. J.; Ellis, D. E.; Ros, P. *Chem. Phys.* **1973**, *2*, 41.
(19) Baerends, E. J.; Ros, P. *Int. J. Quantum Chem.* **1973**, *2*, 42.
(20) Baerends, E. J.; Ros, P. *Chem. Phys.* **1973**, *2*, 51.
(21) Boerrigter, P. M.; te Velde, G.; Baerends, E. J. *Int. J. Quantum Chem.* **1988**, *33*, 87.
(22) te Velde, G.; Baerends, E. J. *J. Comput. Phys.* **1992**, *99*, 84 and references therein.
(23) Vosko, S. H.; Wilk, L.; Nusair, N. *Can. J. Phys.* **1980**, *58*, 1200.
(24) Becke, A. D. *Phys. Rev. A* **1988**, *38*, 3098.
(25) Perdew, J. P. *Phys. Rev. B* **1986**, *33*, 8822.

to the core Mn,3p−O,2p overlap contributions. The large energy scattering of the strictly, t_{1g},t_{2u}, and approximately a_{1g},t_{1u}Mn−O nonbonding orbitals does indicate that there is considerable amount of ligand−ligand and crystal field interaction. The a_{1g} orbital which is O,2p−O,2p bonding (but otherwise Mn−O nonbonding) is strongly stabilized by O,2p−O,2p interactions. Comparing the orbital energies of the MO_6^{8-} clusters with O_h and D_{3d} symmetries, it follows that the trigonal field leads to a large splitting of the t_{1g}, t_{2g}, and t_{2u}O,2p orbitals. This is mainly due to O,2p−O,2p interligand overlap and explains the small trigonal field acting on the t_{2g}(3d) orbitals. The direct overlap between the 3d orbitals centered at neighboring Mn^{IV} ions gives rise to a large variation of the energies of the t_{2g}(3d) orbitals and produces a much smaller effect on the e_g orbital energies (cf. the corresponding energy ranges: 2.8 and 0.5 eV, denoted by Mn-t_{2g} and Mn-e_g, respectively, in Figure 3a).

III.1.2. Charge Transfer (CT) Energies and Electronic Hopping in $Mn^{IV}_7O_{14}$. In the studies thus far, the electronic structure of $Li_xMn_2O_4$ and other electrode materials were treated in terms of band theory,[10−15] assuming delocalized electrons of the partly filled 3d shell. The electronic properties of TM oxides are governed by charge transfer (CT) and electron hopping. In the case of so-called Mott−Hubbard insulators the energy gap is the energy needed to transfer one electron from one TM to another TM, i.e., in the case of Mn_2O_4 to go from a Mn^{IV}−Mn^{IV} to a Mn^{III}−Mn^{V} configuration (eq 4). The Hubbard energy U can be expressed by eq 5, where I and A are the ionization potentials and electronic affinity of Mn^{IV} in its oxide surrounding.

$$U = E(Mn^{III}-Mn^{V}) - E(Mn^{IV}-Mn^{IV}) \quad (4)$$

$$U = I(Mn^{IV}) - A(Mn^{IV}) \quad (5)$$

Another kind of CT is from O^{2-} to Mn^{IV}, leading to a $Mn^{III}L$ (L = hole on O^{2-}) configuration (eq 6).Quite analogous to U, the energy Δ is related to the ionization potential of O and the electronic

$$\Delta = E(Mn^{III},L) - E(Mn^{IV}) \quad (6)$$

affinity of Mn^{IV} (eq 7). CT fluctuations $d_1^n d_2^n \rightarrow d_1^{n+1} d_2^{n-1}$ are less favorable due to interelectronic

$$\Delta = I(O^{2-}) - A(Mn^{IV}) \quad (7)$$

repulsion, though kinetic energy is gained via electronic delocalization and covalency. The later effect is accounted for by the intraatomic matrix element t, i.e., the hopping integral, which provides also a measure of the d bandwidth W (eq 8), where Z is the number of nearest neighbor Mn atoms (for spinel, $Z = 6$).

$$W = Zt \quad (8)$$

If $W/2 > U$, the delocalization will overcompensate the loss in energy due to the electronic repulsion U. For the opposite limit, i.e., $W/2 < U$, the electrons are localized at different sites thus minimizing the on-site repulsion. In what follows we propose a recipe allowing to extract values for t, Δ, and U from DFT cluster calculations. Thus, we shell see that it is this localized description which provides a better starting point for a realistic modeling of the electronic structure and electronic transport behavior of the Mn^{IV}/Mn^{III} oxides.

III.1.2.1. Mn−Mn and Mn−O Hopping Integrals. We analyzed the energies of DFT orbitals with dominant 3d

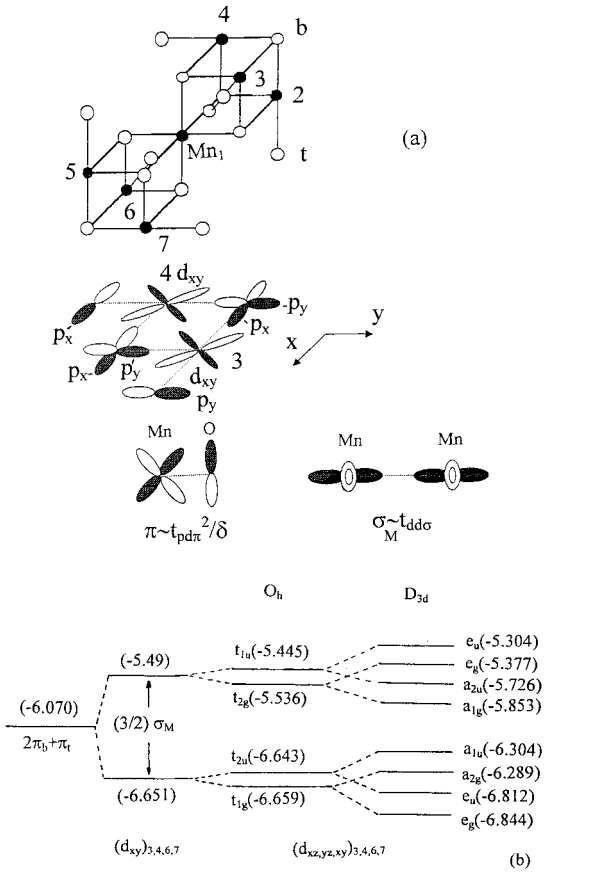

Figure 4. Extended AOM treatment of the Mn_7O_{14} cluster: (a) parameter definitions and coordinate orientations, (b) orbital correlation diagram illustrating the effects of the trigonal and of the cubic ligand fields and of the direct Mn−Mn overlap on the orbital levels.

character in terms of an effective Hamiltonian (h_{eff}),[26,27] constructed in such a way that, when acting on the subspace of the d orbitals, it produces the same orbital energies as given by the DFT calculation of the Mn_7O_{14} cluster. Then, by using perturbation theory, the matrix elements of h_{eff}, $(d_1|h_{eff}|d_2)$ are expressed in terms of angular overlap model parameters for optimally aligned orbitals of σ and π type for Mn−O(denoted hereafter by σ, π) and Mn−Mn(σ_M,π_M) and angular functions $F(\theta,\varphi)$ depending on the angular geometry of the cluster. Orbital and parameter definitions are illustrated in Figure 4a. The application to the $Mn_7O_{14}^-$ cluster allows us to deduce Mn−Mn hopping integrals from a fit of AOM energy expressions to DFT orbital energies. For the sake of illustration we adopt axial geometry for Mn_7O_{14} (Figure 4a) and account for octahedral and trigonal symmetries in a second step. The AOM matrix for the d_{xy}^3−d_{xy}^4 pair of orbitals (eq 9) consists of diagonal energies with contributions from two bridging ($2\pi_b$), one terminal (π_t) Mn−O bond and the direct Mn−Mn interaction term, $(-3/4)\sigma_M$. The same matrix also pertains to the pair of orbitals d_{xy}^6−d_{xy}^7, related to the d_{xy}^3−d_{xy}^4 pair via an inversion center. In addition, eight more d_{xz},d_{yz} orbitals are involved, generated from $d_{xy}^{3,4,6,7}$ via rotation arround the C_3 axis,

$$\begin{array}{c} \begin{matrix} d_{xy}^{\,2} & d_{xy}^{\,4} \end{matrix} \\ \begin{bmatrix} 2\pi_b+2\pi_t & -(3/4)\sigma_M \\ -(3/4)\sigma_M & 2\pi_b+2\pi_t \end{bmatrix} \end{array} \quad (9)$$

(26) Atanasov, M.; Schmidtke, H.-H. *Chem. Phys.* **1988**, *124*, 205.
(27) Atanasov, M.; Angelov, S. *Chem. Phys.* **1991**, *150*, 383.

Table 1. Energies of Mn → Mn and O → Mn Charge Transfer and Electronic Hopping as Deduced from DFT Calculations on the Mn_7O_{14} Extended Cluster

orbital CT parameters and O → Mn CT energies, Δ	Mn → Mn energies, *U*	electron hopping energies, *t*
δ_{t2g} =0.99 eV	$U_{a1g(t2g)} = 6.54$ eV	Mn → Mn:
$\delta_{eg} = 1.90$ eV	$U_{eg(t2g)} = 7.23$ eV.	$t_{2g} = 0.58$ eV
$\Delta_{t2\,g} = 6.87$ eV[a]	$U_{eg(eg)} = 6.30$ eV	$t_{eg} = 0.11$ eV
$\Delta_{eg} = 7.19$ eV	$U_{2p-2p} = 0.68U_{3d-3d}$	O → Mn:
		$t_{2g}' = 2t_{pd\pi} = 0.53$ eV
		$t_{eg}' = \sqrt{3}t_{pd\sigma} = 3.52$ eV

[a] Calculated using a value of $U_{t2\,g} = (1/3)[U_{a1\,g(t2\,g)} + 2U_{eg(t2\,g)}]$ (see eq 13).

by a cyclic permutation $x \rightarrow y \rightarrow z$. This results in an (accidental) 6-fold degeneracy of each eigenvalue in eq 9 which undergoes additionally splitting, however, due to the octahedral (O_h) and trigonal (D_{3d}) ligand fields. A correlation energy diagram based on our DFT results is illustrated in Figure 4b. With ascending symmetry, from D_{3d} to O_h, an estimate of the effective parameter for the $t_{2g}-t_{2g}$ hopping is possible [$t_{t2g} = (3/4)\sigma_M = 0.58$ eV]. A much smaller value for the e_g-e_g hopping parameter ($t_{eg} = 0.108$ eV) results from a similar treatment if one includes the $e_g(\sigma)$ orbitals (see Appendix).

How do (*t*) values depend on the choice of cluster and the adopted basis set? If we keep to the same basis set (section II) and take a $[(H_2O)_4Mn^{IV}(\mu\text{-}O)_2Mn^{IV}(H_2O)_4]^{+4}$ cluster a value of *t* for σ orbitals is calculated[28] [$t_\sigma = 0.5\,(t_{x^2-y^2} + t_{z^2}) = 0.122$ eV], quite close to our t_{eg} parameter (0.108 eV). t_σ increases, however, to 0.147 eV if ligand basis functions of double-ζ, instead of triple-ζ, quality are used.

The partitioning scheme, based on second-order perturbation theory described above, does not allow us to extract the Mn−O hopping energies (*t*) from angular overlap modeling of our DFT data. However, an estimate for *t* as well as for the O → Mn orbital CT energy (δ) is still possible. Indeed, from the difference between the antibonding (a) and bonding (b) energies of the e_g and t_{2g} orbitals, Δ*E*, and the percentage (c) of Mn(O) orbital character to *a*(*b*) as given by our DFT data, the effective parameters (δ) and (*t*) of the matrix (eq 10)

$$\begin{bmatrix} \text{Mn} & \text{O} \\ \text{O} & t \\ \text{t} & -\delta \end{bmatrix} \tag{10}$$

can be easily reconstructed by solving the set of equations:

$$\delta^2 - 2(1 - c/100)\Delta E\delta + \Delta E^2(1 - 2c/100) = 0$$

$$t = (1/2)(\Delta E^2 - \delta^2)^{1/2} \tag{11}$$

Matrix 10 is the 2 × 2 Hamiltonian for the $Mn^{IV}O_6^{8-}$ cluster with compensating point charges, written in the basis of the metal 3d and ligand 2p functions of $\sigma(e_g)$ and $\pi(t_{2g})$ symmetry.

Substituting the values of Δ*E* and *c* obtained in the DFT calculation (t_{2g}, 1.457 eV, 16%; e_g, 7.302 eV, 37%), we obtain values for δ and *t* (cf. Table 1, where $t_{pd\sigma}$ and $t_{pd\pi}$ denote standard matrix elements). The results show a rather large σ but small π hopping energy. The parameter δ is closely related to the O → Mn charge-transfer energy Δ (see below).

III.1.2.2. The Mn → Mn and O → Mn CT Energies *U* and Δ. In DFT, the Mn → Mn CT energies U_i for orbitals (i) can be approximated with the second derivative of the total energy E_{tot} with respect to the occupation number n_i, or alternatively, with the fist derivative of the orbital energy ϵ_i:[29]

$$U_i = \partial^2 E_{tot}/\partial^2 n_i = \partial \epsilon_i/\partial n_i \tag{12}$$

Thus, the values for the parameters U_i corresponding to the d orbitals of the $Mn^{IV}O_6^{8-}$ cluster (Table 1) are calculated using finite differences.

Within the Slater's transition state method,[29] the parameters Δ_{eg} and Δ_{t2g} for CT between O,2p($1e_g$, $2t_{2g}$, $1t_{1g}$) and Mn,3d-($2e_g$,$2t_{2g}$) orbitals are given by eq 13

$$\Delta_i = \delta_i + (1/2)U_i(3d) + (1/2)U_i(2p) \tag{13}$$

Substitution of δ (from eq 11) and *U* (eq 12) as well as $U(p)/U(d) = 0.68$[30] yields the values of Δ_{eg} and Δ_{t2g} values listed in Table 1.

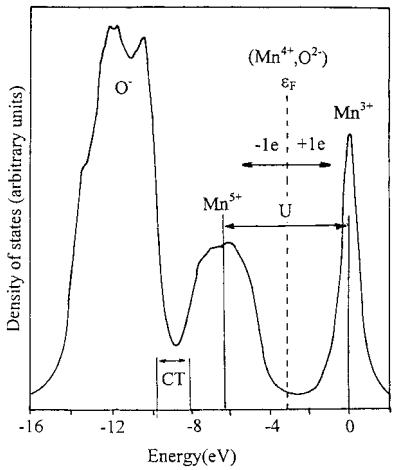

Figure 5. Total energy diagram illustrating the density of states resulting from the removal/addition of one electron from/to Mn_2O_4. The *U* energy and the onset of the CT absorption transitions are indicated.

III.1.2.3. Electronic Structure of Mn_2O_4 Spinel. We are now in a position to draw an energy diagram using the CT energies *U* and Δ and the hopping integrals given in Table 1 for Mn_2O_4. Thus, in Figure 5 we plot the density of states vs the total energy of a system with one additional hole ($Mn_2O_4^+$) and one additional electron ($Mn_2O_4^-$) as compared to the ground-state energy of Mn_2O_4 as reference (ϵ_F). This curve results from a single particle (Hartree−Fock) solution of the Hubbard Hamiltonian. The density of states for the system with one additional 3d hole or electron are calculated taking translational symmetry into account, while those corresponding to an O,2p ionized final state have been approximated using the results of the DFT calculation on the Mn_7O_{14} cluster.[31] The

(28) Atanasov, M. Unpublished results, in preparation for publication.

(29) Slater, J. C. *The Self-Consistent Field for Molecules and Solids*; McGraw-Hill Book Co.: New York, 1974. In deriving expressions for the charge transfer parameters Δ_i using this approach the attraction between the ligand 2p hole and the metal 3d-electron [given by a $-U_i(2p-3d)$ term] has to be omitted. Likewise, the values of U_i pertain to discussions of the energy gap which separates bound states from the free charge carriers. For the determination of the parameters U_i, also see: Neshev, N. M.; Proinov, E. I. *J. Mol. Catalysis* **1989**, *54*, 484.

(30) Eskes, H. Ph.D. Thesis, RU Groningen, The Netherlands 1992.

(31) The density of states is calculated by means of the histogram method (Brust, J. *Methods of Computational Physics*; Academic Press: New York; Vol. 8, p 52.) using the formula $D(E_i) = \Sigma_{(n)}\,\Sigma_{(k)}\delta^{\Delta E}[E_i - E_n(k)]$, where the summation *n* extends over the energy bands and *k* over a number of selected points in the Brillioin zone. The Kronecker symbol $\delta^{\Delta E}[E_i - E_n(k)]$, equals 1 if $|E_i - E_n(k)| \le \Delta E/2$ and 0 otherwise, where the interval $\Delta E = E_{i+1} - E_i$ is chosen to be small compared to the width of the band. In calculating the density of states of the correlated d bands we follow the formalism described in detail by Hubbard, J. *Proc. R. Soc. A* **1963**, *276*, 238.

zero-density of states for hole and electrons at the Fermi level is typical for insulating oxides and we can unambiguously assign Mn_2O_4 to this category. The conductivity gap is of Mott−Hubbard type (4.2 eV). It results from the energy needed to create one t_{2g} hole on a given Mn^{IV} and to put one e_g electron on a different Mn^{IV}. In addition one has to overcome the attraction between them, the two contributions (6.3 eV) being reduced by a negative energy term (−2.07 eV) due to the finite 3d bandwidths, i.e., 1.74 eV for the lower one and 0.33 eV for the upper bands (cf. Figure 5).We can, roughly, identify the lowest CT transition energy in Mn_2O_4 with the energy difference between the bottom and the top of the t_{2g} and O,2p band (for hole states), respectively (1.7 eV). A CT gap with this energy would give rise to intense CT transitions extending from the near-IR to the optical region. This explains the dark colors of the Mn_2O_4 spinel and of the other related oxides. The onset of the CT band will be shifted to the blue, however, if Mn^{IV} enters as an impurity ion into lattices at octahedral MO_6 sites. This shift is expected to amount the half-width of the 3d band (1.74 eV), thus increasing the optical CT gap from 1.7 to 3.44 eV and opening a spectral region for weaker crystal field excitations in visible spectral region. Mn^{IV} in such systems, such as Mn^{IV}:YAG, has indeed been characterized and the crystal field excitations as well as the corresponding parameters are well documented.[32]

It should be noted that, despite the large value of the O → Mn hopping energy (t_{eff} = 3.52 eV), the e_g levels broaden weakly into a band. This is because Mn^{IV} e_g(3d) orbitals are bridged by O^{2-} 2p orbitals, which are mutually orthogonal (the Mn−O−Mn bridging angle β is close to 90°). Thus, the widths of the 3d and O → Mn bands are determined mainly by Mn−Mn and O−O overlap, respectively.[33]

The energy diagram in Figure 5 accounts for electronic correlation and differs strongly from the description which results from spin restricted DFT band calculation of Mn_2O_4 spinel.[34] In this case a nonzero density of states at the Fermi level ϵ_F is obtained, in contrast to experiment. A spin-unrestricted calculation leads to a gap, but it is of exchange, rather than of correlation type. Finally, a spin-unrestricted band calculation of $LiMn_2O_4$ yields again nonzero density of states at ϵ_F, implying a metal, in contrast to experiments which show $LiMn_2O_4$ to be a polaronic semiconductor. The comparison shows once more[35] that a localized, rather than a spin restricted band description, is the method of choice, thus justifying the cluster approach.

III.2. Vibronic Coupling in a $Mn^{III}O_6$ Octahedron. The addition of one electron into the antibonding $2e_g$ orbitals of the $Mn^{IV}O_6$, leads to an elongation of the Mn−O bond due to the Mn−O antibonding interaction which is stronger in the σ type $2e_g$ compared to the π $2t_{2g}$ orbitals. The changes in geometry can be described in terms of a shift along the α_{1g} MnO_6 octahedral mode (Figure 6a) which increase uniformly all Mn−O bond lengths. In addition, the doubly degenerate ground state $^5E_g(t_{2g}^3e_g^1)$ of $Mn^{III}O_6$ is vibronically unstable. It splits by distortions along the normal mode of E symmetry (ϵ_g) leading to lower D_{4h} and D_{2d} symmetries for the two components Q_θ and Q_ϵ, respectively. The energy gain is the Jahn−Teller (JT) stabilization energy. These two modes are illustrated in Figure 6b. For Mn^{III} in an octahedral ligand field the distorting forces are such as to lower the energy via a tetragonal elongation (D_{4h}) of the octahedron (see below). The superposition of this distortion with the D_{3d} site symmetry of the Mn site leads to C_{2h} symmetry. However the presence of one Li atom at the 8a spinel site lowers the symmetry further to C_s. To quantify these changes of the ground-state energies for the $Mn_7O_{14}^-$ and for the Mn_7O_{14} clusters, we have placed the extra electronic charge at the cluster $2e_g$(3d) orbital of the central MnO_6 subunit. These two different sets of calculations on this cluster, in D_{3d} and C_s symmetries, allow us to analyze the geometric distortions in terms of vibronic coupling constants for the α_{1g} and ϵ_g modes.

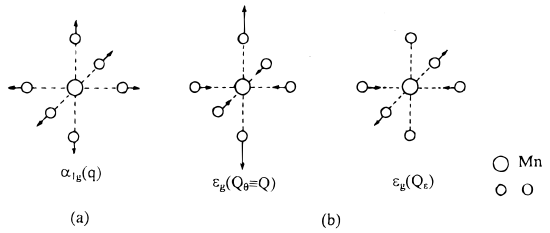

Figure 6. Vibrational modes involved in the vibronic coupling due to the $2e_g$ electron of Mn^{III}. (a) α_{1g} mode, (b) Jahn−Teller active $\epsilon_g\theta$ and ϵ modes.

Table 2. DFT Total Energies (E_{tot} in EV) of Mn_7O_{14} (Mn_1^{IV}, $2t_{2g}^3$, O_h Notation and $Mn_7O_{14}^-$(Mn_1^{III}, $2t_{2g}^3 2e_g^1$) Clusters in D_{3d} Symmetry vs the Equilibrium Mn^{IV}−O and Mn^{III-}−O Distances (R_{ML} in ångstroms)

R_{ML}	2.005[a]	2.211[b]
δR	0.0	0.206
$q_o = \sqrt{6}.\delta R$	0.0	0.504
$E_{tot}(Mn_7O_{14})$	−143.036 135[a]	−142.845 564
$\Delta E_{tot}(Mn_7O_{14})$	0.0	0.190
$E_{tot}(Mn_7O_{14}^-)$	−146.156 022	−146.384 209[b]
$\Delta E_{tot}((Mn_7O_{14}^-)$	0.0	−0.228

[a] DFT geometry optimized geometry for Mn_7O_{14}. [b] DFT optimized geometry for $Mn_7O_{14}^-$.

III.2.1. α_{1g} Distortion. The total energies of the Mn_7O_{14}-(Mn_1,$2t_{2g}^3$) and $Mn_7O_{14}^-$($2t_{2g}^3 2e_g^1$) clusters in D_{3d} symmetry are listed in Table 2. The energies of the Mn_7O_{14} and $Mn_7O_{14}^-$ clusters have been calculated at two different geometries, corresponding to the optimal geometry of Mn_7O_{14} and $Mn_7O_{14}^-$ as obtained from the DFT calculations. Adding one extra electron to the antibonding Mn_1,$2e_g(Mn_1)$ orbital leads to an elongation of the Mn_1−O distances of 0.206 Å, while leaving the other structural parameters almost unchanged (Figure 7a). We neglect these latter geometry changes and take the equilibrium Mn^{IV}−O distance as a reference. The dependence of the total energies of the $Mn_7O_{14}^-$ and Mn_7O_{14} clusters on the shift q along the α_{1g} mode are given by eq 14 where k and k' are the harmonic force constants and a the linear vibronic coupling constant, i.e.:

$$\Delta E_{tot}(Mn_7O_{14}^-) = (^1/_2)kq^2 + aq$$
$$\Delta E_{tot}(Mn_7O_{14}) = (^1/_2)k'q^2 \qquad (14)$$

From the calculated value of the displacement between the $Mn_7O_{14}^-$ and Mn_7O_{14} equilibrium geometries q_o, the energy stabilization $\Delta E_{tot}^o(Mn_7O_{14}^-)$ and the energy increase $\Delta E_{tot}^o(Mn_7O_{14})$ (Table 2) the parameters k,a and k' are calculated

(32) Hartung, S. Ph.D. Thesis, Hamburg, Germany, Bern, Switzerland, 1997.

(33) The situation can change strongly when going to $CaMn^{IV}O_3$ with perowskite structure, however, where Mn−O−Mn bridging angles range between 150° and 180°. This leads to much larger band widths for the O → Mn CT states (W_{eg} = 6.48−8.64 eV) and can change from insulating to metallic behaviour in the Mn^{IV}/Mn^{III} mixed valence compounds. This might have crucial consequences for the giant magnetoresistance system $La_{0.8}Ca_{0.2}MnO_3$ with remarkable properties which are not understood yet.

(34) Barras, J.-L.; Daul, C. A.; Deiss, E.; Benco, L.; Atanasov, M. *Theochem*. Submitted for publication.

(35) Zaanen, J.; Sawatzky, G. A. *Canad. J. Phys.* **1987**, *65*, 1262. Zaanen, J.; Sawatzky, G. A. *J. Solid State Chem.* **1990**, *88*, 8.

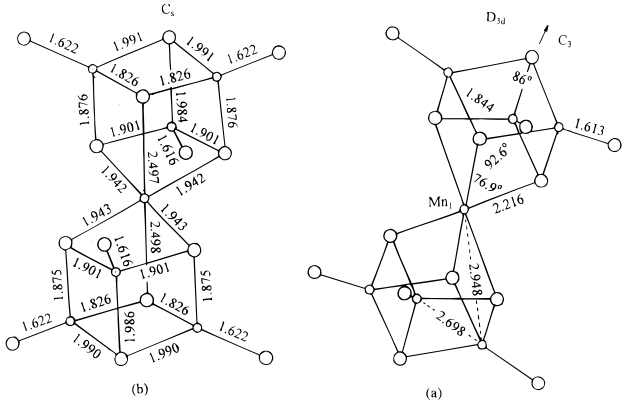

Figure 7. Selected bond distances and bond angles of the optimized DFT geometry for the $Mn_7O_{14}^-$ clusters with one active $2e_g(Mn^{III})$ electron at the MnO_6^q central subunit. (a) $2t_{2g}^3 2e_g^1$: D_{3d} geometry optimization. (b) $2t_{2g}^3 2e_g(d_{z^2}^1)$: C_s geometry optimization.

Table 3. Force Field Constants, Linear Vibronic Coupling Parameters, and Vibronic Stabilization Energies (E_{vib}) of $Mn^{III}O_6$ in Mn_7O_{14}

$\alpha_{1\,g}(q)$ Mode, D_{3h} Symmetry

energy: $\Delta E_{tot}(Mn_7O_{14}^-) = (^1/_2)kq^2 + aq \qquad \Delta E_{tot}(Mn_7O_{14}) = (^1/_2)k'q^2$

parameters: $k = 1.795$ eV/Å^2, $a = -0.905$ eV/Å, $k' = 1.496$ eV/Å^2.

$E_{vib} = -(^1/_2)a^2/k = -0.228$ eV

$\alpha_{1\,g}(q) + \epsilon_g(Q)$ Modes: C_s Symmetry

energies: $\Delta E(2t_{2g}^3 d_{z^2}^1) = (^1/_2)kq^2 + (^1/_2)KQ^2 + aq + AQ + lqQ$

$\Delta E(2t_{2g}^3 d_{x^2-y^2}^1) = (^1/_2)kq^2 + (^1/_2)KQ^2 + aq - AQ - lqQ$

parameters: $k = 1.645$ eV/Å^2, $a = -0.905$ eV/Å

$K = 1.206$ eV/Å^2, $A = -0.966$ eV/Å

$l = 0.644$ eV/Å^2

energy: $\Delta E(2t_{2g}^3 d_{z^2}^1) = (^1/_2)k'q'^2 + (^1/_2)K'Q'^2 + a'q' + A'Q'$

parameters: $k' = 0.746$ eV/Å^2, $a' = -0.26$ eV/Å

$K' = 2.108$ eV/Å^2, $A' = -1.298$ eV/Å

$E_{vib} = -(^1/_2)a'^2/k' - (^1/_2)A'^2/K' = -0.045 - 0.400 = -0.445$ eV

using the relations of eq 15. These results are listed in Table 3. Note that, for the α_{1g}Mn−O stretching mode, in the relations

$$q_o = -a/k$$

$$\Delta E_{tot}{}^o(Mn_7O_{14}^-) = -(^1/_2)kq_o{}^2$$

$$\Delta E_{tot}{}^o(Mn_7O_{14}) = (^1/_2)k'q_o{}^2 \qquad (15)$$

the force constants k and k' are not equal. k refers to Mn_7O_{14} and k' to $Mn_7O_{14}^-$. In fact, k gets larger when going from Mn^{IV} to Mn^{III}. The cause for this change is possibly due to the rigidity on the MnO_6 subunit imposed by the surrounding Mn_{2-7} polyhedra when increasing the equilibrium bond length of Mn_1−O bond length from Mn^{IV} to Mn^{III}. However, this effect is not very large and for the sake of simplicity in the further discussion we shall neglect this difference and take an average k value of 1.645 eV/Å^2.

III.2.2. Jahn−Teller Distortions and the Interplay between the $\alpha_{1\,g}$ and ϵ_g Modes. The geometry optimization of the $Mn_7O_{14}^-$ cluster with one extra d_{z^2} electron in C_s symmetry leads, as expected, to a tetragonally elongated MnO_6 octahedron with distinctly different axial (2.497 Å) and equatorial (1.942 Å) Mn−O bond lengths (Figure 7b). The average (2.127 Å) and the "axial" (2.497 Å) bond distances are larger than experimentally reported (2.07 and 2.30 Å in $Li_2Mn_2O_4$[36]).

The reason may be the fact that electronic localization is more pronounced in clusters than in solids with extended M−O−M networks. It increases the vibronic coupling and thus causes a larger difference between axial and equatorial bond distances. Another reason might be anharmonicity which tends to increase this difference as well. It becomes smaller on going from clusters to an extended arrays.[37] Finally, the approximations inherent in our DFT calculations, the restricted basis set (see section II) might also contribute to larger Mn−O bond distances [compare $R(Mn^{IV}-O)$: 1.912 Å (exptl) and 2.005 Å (calcd)].

The deviation from the equilibrium geometries of Mn_7O_{14} to $Mn_7O_{14}^-$ leads to a lowering of the total energy of $Mn_7O_{14}^-$ from −146.1260 [38] to −146.5714 eV. This stabilization energy of −0.445 eV results from the geometric relaxation of the $Mn_7O_{14}^-$ cluster due to contributions from both the α_{1g} and ϵ_g modes. As expected, the energy lowering is larger as compared to the one (−0.228 eV) obtained by excluding the action of the ϵ_g JT mode (constraint optimization in D_{3d} symmetry). If we take the z axis as the C_4 axis of the elongated octahedron (D_{4h} pseudosymmetry), a shift along the Q_θ component of the ϵ_g mode of 0.641 Å is obtained using eq 16 and the Mn−O bond distances (R_{ax}, 2.497 Å and R_{eq}, 1.942 Å). Here ΔR_{ax} and ΔR_{eq} are the deviations of the axial and of the equatorial bond lengths

$$Q_o \equiv Q_\theta{}^o = (2/\sqrt{3})\,(\Delta R_{ax} - \Delta R_{eq}) \qquad (16)$$

from their average value of $R = 2.127$ Å. The increase of the average Mn−O bond distance in going from Mn^{IV} to Mn^{III} calculated by DFT, i.e., 0.12 Å, agrees well with the difference of the corresponding ionic radii (0.115 Å[39]) as well as with a recent EXAFS study on $LiMn_2O_4$ (0.1 Å[40]). It should be noted that the average Mn−O bond length for the $Mn_7O_{14}^-$ cluster (2.127 Å) when optimized in C_s symmetry differs from the optimal D_{3d} value (2.211 Å). This implies a displacement along the α_{1g} mode of $q_o = 0.299$ Å if one accounts for the JT effect and of $q_o = 0.504$ Å if one neglects the JT effect. Apparently, there is an interplay between the α_{1g} and the ϵ_g modes and we are going now to analyze this more thoroughly. Without loss of generality, we can confine our treatment to tetragonally elongated ($Q \equiv Q_\theta > 0$) and compressed ($Q < 0$) octahedra ($Q_\epsilon = 0$). Taking again the equilibrium Mn−O bond distance ($R_{Mn-O} = 2.005$ Å) as reference ($q = Q = 0$) and restricting our analysis to linear vibronic coupling terms only, the total energy of the doubly degenerate $[2t_{2g}^3 2e_g(d_{z^2}, d_{x^2-y^2})^1]$ configuration of MnO_6 is given by

$$\Delta E(2t_{2g}{}^3 d_{z^2}{}^1) = (^1/_2)kq^2 + (^1/_2)KQ^2 + aq + AQ + lqQ$$

$$\Delta E(2t_{2g}{}^3 d_{x^2-y^2}{}^1) = (^1/_2)kq^2 + (^1/_2)KQ^2 + aq - AQ - lqQ \qquad (17)$$

where (k,K) and (a,A) are the harmonic force and linear vibronic coupling constants, for the α_{1g} and ϵ_g modes, respectively. l is the bilinear coupling constant, which describes the α_{1g} and ϵ_g mixing. In eq 17, second-order JT coupling, which adds (for d_{z^2}) and subtracts (for $d_{x^2-y^2}$) a term of the form BQ^2 (B is the second-order vibronic constant), has been neglected. Such terms are 1 order of magnitude smaller than the linear terms and they

(36) Goodenough, J. B.; Thackeray, M. M.; David, W. I. F.; Bruce, P. G. *Rev. Chim. Miner.* **1984**, *21*, 435.

(37) Deeth, R. J.; Hitchmann, M. A. *Inorg. Chem.* **1986**, *25*, 1225.

(38) Note a small difference between the energies of $Mn_7O_{14}^-$ calculated using the same geometry (optimized for Mn_7O_{14}) but imposing different symmetries − D_{3h}(−146.1560 eV) and C_s(−146.1260 eV).

(39) Shannon, R. D. *Acta Crystallogr. A* **1976**, *32*, 751.

(40) Shiraishi, Y.; Nakai, I.; Tsubata, T.; Himeda, T.; Nishikawa, F. *J. Solid. State. Chem.* **1997**, *133*, 587.

do favor the d_{z^2} ground state. Their origin has been discussed in detail elsewhere.[41,42] Focusing on a d_{z^2} ground state, we can minimize eq 17 with respect to q and Q to yield expressions for the JT coupling (K,A) and the mixing parameter (l) (eq 18). We are now in a position to calculate K, A, and l, i.e.:

$$l = -(kq_o + a)/Q_o$$
$$K = (kq_o^2 + 2aq_o - 2.\Delta E_{tot}^o)/Q_o^2$$
$$A = -KQ_o - lq_o \quad (18)$$

starting from the DFT values for the $Mn_7O_{14}^-$ equilibrium displacements, i.e., q_o(0.299 Å), Q_o(0.641 Å), and from the stabilization energy ΔE_{tot}^o = -0.445 eV and adopting the k and a values for α_{1g} as resulting from the D_{3d} geometry optimization (section III.2.1). A summary of vibronic coupling parameters values for the $Mn_7O_{14}^-$ cluster is given in Table 3. Accounting for the $\alpha_{1g}-\epsilon_g$ mixing term (l = 0.644 eV/Å^2) results in a smaller vibronic stabilization energy (−0.445 eV) as compared to the value which results (−0.636 eV), if one takes separate contributions from the α_{1g} (−0.249 eV) and ϵ_g (−0.387 eV) modes, neglecting their interaction. The cause for this difference is of elastic origin. This can easily be seen by diagonalizing the force field matrix (eq 19), thus transforming from q and Q to new vibrational modes q' and Q' [and corresponding force constants (k',K') and vibronic coupling parameters (a',A')] given in eq 20,

$$\begin{bmatrix} k & l \\ l & K \end{bmatrix} \quad (19)$$

and eliminating in this way the bilinear term lqQ (eq 21).[43] The results (Table 3) show the

$$Q' = 0.84q + 0.58Q$$
$$q' = -0.58q + 0.81Q \quad (20)$$

$$E(2t_{2g}^3 d_{z^2}^1) = (1/2)k'q'^2 + (1/2)K'Q'^2 + a'q' + A'Q' \quad (21)$$

prevalent activity of the JT mode (Q') with larger A' and K' values. However, when going to the new basis, K' increases more than A', thus reducing the total stabilization energy from −0.636 to −0.445 eV. On the basis of the vibronic stabilization energy ΔE and of the ratio $\lambda = \Delta E/h\nu$, $h\nu$ being the vibrational energy, we can deduce, within the inherent cluster approximation, that MnO_6 represents a case of strong (Q', $h\nu$ = 193 cm^{-1}, λ = 16.7) to moderate (q', $h\nu$ = 113 cm^{-1}, λ = 3.2) vibronic coupling.

III.3. A Small Polaron Model and the Electronic Transport in the Mn^{IV}/Mn^{III} Mixed Valent $Li_xMn_2O_4$. The doping of Li into the Mn_2O_4 spinel structure leads to a reduction of an equivalent amount of Mn^{IV} ions to Mn^{III} with one extra $2e_g(\sigma)$ electron. The associated change of the Mn−O bond lengths and energy lowering tends to trap this electron on a given Mn^{III} site. On the other hand, the stabilization due to a gain of kinetic energy by delocalization of the electron in a band will be opposed to the forces distorting the ionic surrounding of Mn^{III}. As is shown by our DFT calculations of the $Mn_7O_{14}^-$ cluster, the vibronic stabilization energy (−0.445 eV) owing to the $2e_g$ electron exceeds the energy of electron hopping (−0.108 eV) from a Mn^{III} to a Mn^{IV} site and is sufficient to cause valence trapping, thus localizing the charge carrier on a given Mn^{III} site (small polaron formation). Small polarons can move from site to site by a thermally activated hopping mechanism.[44] In the following we will explore their effect on the electronic conductivity and compare our results with data from experiment. Let us first consider the high Li-doping case, such as that in $Li_xMn_2O_4$ ($x \geq 1$), and assume a static JT distortion. It splits the doubly degenerate e_g orbital and hence a single orbital approximation is reasonable. Second order JT coupling does stabilize tetragonally elongated octahedra ($d_{z^2}^1$ HS ground state), which, in the case of $LiMn_2O_4$, at temperatures below 280 K does orient them parallel to each other giving rise to a phase transition.[45] When adopting a single $d_{z^2}^1$ type ground state we return to eq 21 for its energy. This equation can be further reduced to a form which includes the vibronic coupling of the electronic state to the effective mode q_1 and to a second mode q_2 for which the linear vibronic coupling constant vanishes (eq 22). q_1 and q_2 are related to q' and Q' as

$$E(2t_{2g}^3 d_{z^2}^1) = (1/2)q_1^2 + Vq_1 + (1/2)q_2^2$$
$$q' = (a'/k'V)q_1 - [A'/(k'K')^{1/2}\ V]q_2$$
$$Q' = (A'/K'V)q_1 + [a'/(k'K')^{1/2}V]q_2$$
$$V = (a'^2/k' + A'^2/K')^{1/2} \quad (22)$$

given in eq 22.The force field constant (k_1) of the effective interacting mode(static JT effect) reads

$$k_1 = [(a'^2 + A'^2)k'K']/(a'^2K' + A'^2k') \quad (23)$$

Let us consider now a dimer, consisting of two Mn ions, Mn_a and Mn_b surrounded with the oxygen atoms, i.e., a small cluster extracted from the spinel lattice. There are two potential curves with effective interacting modes q_a and q_b corresponding to the states where the extra electron resides on Mn_a or Mn_b (eq 24). Next we consider a vibrational mode x for which

$$E_a = 1/2 q_a^2 + Vq_a$$
$$E_b = 1/2 q_b^2 + Vq_b \quad (24)$$

the elongation of the Mn−O bonds at one center is accompanied by the compression of the corresponding bonds on the other one, i.e.,

$$x = (1/2)(q_a - q_b), \quad q_a = -q_b \quad (25)$$

Combining eq 24 and eq 25 we obtain

$$E_a = (1/2)\, x^2 + Vx$$
$$E_b = (1/2)x^2 - Vx \quad (26)$$

An energy plot using parameters from Table 3 is given in

(41) Yamatera, H. *Acta Chem. Scand. A* **1979**, *33*, 107.

(42) Reinen, D.; Atanasov, M. *Magn. Reson. Rev.* **1991**, *15*, 167 and references therein.

(43) In a similar way, equation for $E(2t_{2g}^3 d_{x^2-y^2}^1)$ can be transformed to q'' and Q'' coordinates with $Q'' = -0.814q + 0.58Q$ and $q'' = -0.58q' - 0.814Q$ and $E(2t_{2g}^3 d_{x^2-y^2}^1) = (1/2)k''q''^2 + (1/2)K''Q''^2 + a''q'' - A''Q''$ with values of k'', K'', a'', A'' equal to k',$K'a'$,A'. However, q'' and Q'' differ from q' and Q'. It is therefore impossible to eliminate the mixed terms lqQ for d_{z^2} and $d_{x^2-y^2}$ at the same time by a single unitary transformation.

(44) Austin, I. G.; Mott, N. F. *Adv. Phys.* **1969**, *18*, 41.

(45) Two different $LiMn_2O_4$ low-temperature structures have been reported. Orthorhombic: Rodriguez-Carvajal, J.; Rousse, G.; Masquelier, C.; Hervieu, M. *Phys. Rev. Lett.* **1998**, *81*, 4660. More recently, tetragonal: Wills, A. S.; Raju, N. P.; Greedan, J. E. *Chem. Mater.* **1999**, *11*, 1510. These results possibly reflect the rather complex relationship between structure and sample nonstoichiometry (x, $Li_{1\pm x}Mn_2O_4$).

Figure 8a. The minimum of each curve occurs for the appropriate distorted configuration giving the difference of equilibrium bond lengths around Mn for Mn^{III} or for Mn^{IV}. For the symmetric configuration ($x = 0$), the curves do cross and show that the system must aquire sufficient energy (the activation energy, $E_a = -0.445$ eV) to reach this point before the electron can move to the other atom. In Figure 8a we present also a plot accounting for the Mn−Mn hoping energy (−0.108 eV) which yields an off-diagonal term mixing the two localized states:

$$\begin{matrix} d_{z^2}(Mn_a) & d_{z^2}(Mn_b) \end{matrix}$$
$$\begin{bmatrix} (^1/_2)x^2 + Vx & t \\ t & (^1/_2)x^2 - Vx \end{bmatrix} \qquad (27)$$

At the crossing point, a stabilized bonding combination is formed which lowers the activation energy from 0.445 to 0.337 eV. The calculated activation energy for electron transfer (0.337 eV) is in reasonable agreement with the value deduced from the conductivity data on $LiMn_2O_4$ (0.4 eV [46]) where a thermally activated, $\sim\exp(-E_a/kT)$, polaronic mechanism of conductivity has been assumed.[47]

Let us now consider another possibility. Neglecting second-order JT coupling, we assume that elongated and compressed octahedra corresponding to d_{z^2} and $d_{x^2-y^2}$ states, being of the same energy are equally probable. We will show that under this condition a path of electronic transfer with very low activation energy results. If we introduce again cluster vibrational modes for the breathing (α_{1g}) mode and the JT mode, x and y, respectively, in the same way as in eq 26 and if we impose, in addition, the conditions

$$q_a = -q_b \qquad \text{and} \qquad Q_a = -Q_b$$
$$x = (^1/_2)(q_a + q_b)$$
$$y = (^1/_2)(Q_a + Q_b) \qquad (28)$$

then the following energy equations corresponding to the four possible localizations of the exceeding electron on Mn_a,Mn_b-(d_{z^2},$d_{x^2-y^2}$) can be derived from the couple of eq 17

$$E(Mn_a^{IV}Mn_b^{III},d_z^2) = -ax - Ay + lxy$$
$$E(Mn_a^{IV}Mn_b^{III},d_{x^2-y^2}) = -ax + Ay - lxy$$
$$E(Mn_a^{III},Mn_b^{IV},d_z^2) = ax + Ay + lxy$$
$$E(Mn_a^{III},Mn_b^{IV},d_{x^2-y^2}) = ax - Ay - lxy \qquad (29)$$

where the harmonic term $(^1/_2)kx^2 + (^1/_2)Ky^2$ has to be added. Moreover, electronic coupling is taken into account (eq 30). Using parameters for Mn_2O_4 from Table 3,

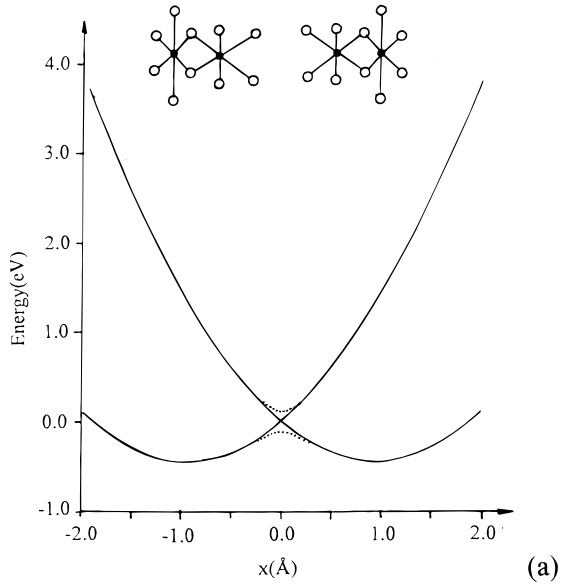

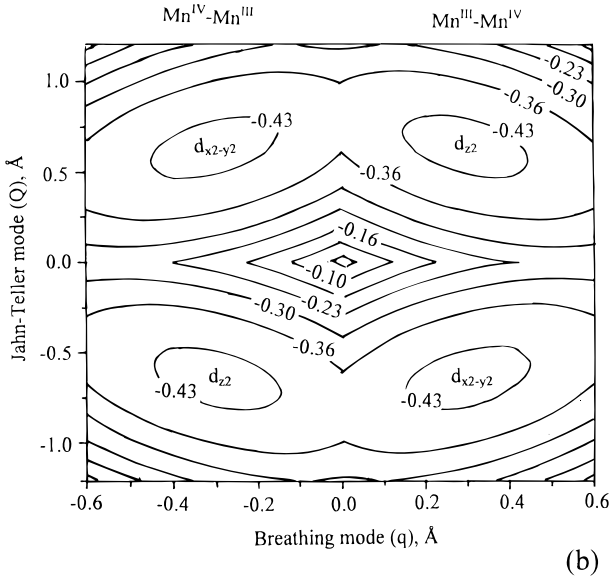

Figure 8. (a) Energy diagram for the small polaron model of $LiMn_2O_4$ with a d_{z^2}, $^5Eg(2t_{2g}^3 2e_g^1)Mn^{III}$ ground state. The upper picture shows a dimer extracted from the Mn_2O_4 spinel. The horizontal coordinate corresponds to the single effective interacting mode (x) which distorts the Mn−O bond lengths as indicated. The two minima correspond to the two possible localizations on Mn_a or Mn_b. Thermal electron transfer requires an activation energy $E_a = 0.445$ eV ($t = 0$, solid lines) and 0.34 eV ($t = 0.11$ eV, dashed lines) needed to distort the ground-state configuration. The parameters used for the plot are those specified in connection with eq 26 (cf. text). (b) Energy contour diagram for a polaronic model for energetically equivalent d_{z^2} and $d_{x^2-y^2}(Mn^{III})$ states and two interacting modes [α_{1g} and the Jahn−Teller active $\epsilon_g(\theta)$]. Parameters used in the plot are those specified in connection with eqs 17 and 29 (cf. text).

$$\langle Mn_a^{IV}Mn_b^{III},d_z^2(d_{x^2-y^2}) \,|h|\, Mn_a^{III}Mn_b^{IV},d_z^2(d_{x^2-y^2})\rangle = t \qquad (30)$$

an energy contour plot is obtained (cf. Figure 8b). In accordance with the four possible localizations of the $2e_g(Mn^{III})$ electron above, four equivalent minima [at (x,y) coordinates (±0.31 Å, ±0.64 Å)] at energy −0.445 eV with respect to the origin (0,0) are calculated. Note the appearance of a low energy path for $Mn^{III} \rightarrow Mn^{IV}$ electronic transfer from a d_{z^2} orbital to a neighboring $d_{x^2-y^2}$ orbital with an activation energy ($E_a = 0.062$ eV at $x = 0$, $y = \pm 0.885$ Å). The polaronic model (vide supra)

(46) Massarotti, V.; Capsoni, D.; Bini, M.; Chiodelli, G.; Azzoni, C. B.; Mozzati, M. C.; Paleari, A. *J. Solid State Chem.* **1997**, *131*, 94.

(47) Holstein, T. *Ann. Phys. NY* **1959**, *8*, 343. An expression for the conductivity by this mechanism is $\sigma = (f/kT)\exp(-E_a/kT)$, $f = N_{el}c(1-c)\nu/a$; c and $(1-c)$ are the relative proportions of the two oxidation states, $c(1-c)$ being the probability that the electron jumps from a given Mn^{III} to a neighbor Mn^{IV} site. a is the lattice constant, ν the vibrational frequency, N_{el} the number of electrons in the elementary cell, and E_a the activation energy. With σ, T, ν, a, and E_a expressed in units of Ω^{-1} cm^{-1}, K, cm^{-1}, Å, and eV, respectively, this equation takes the form: $\sigma = 5.57630 \times 10^3 [N_{el}c(1-c)\,\nu/a]\exp[-E_a/(8.258 \times 10^{-5}T)]$ Inserting values for $c(1-c)$, N_{el}, a, ν, and E_a pertaining to $LiMn_2O_4$ (0.25, 8, 8.045 Å, 189 cm^{-1}, and 0.34 eV, respectively) yields the σ vs T plots in good agreement with experimental conductivity curves in ref 46.

with two modes and energetically equivalent d_{z^2},$d_{x^2-y^2}$ orbitals very probably pertains to $Li_{1+x}Mn_2O_4$ ($x < 0$, dynamic JT regime). Reported smaller values of E_a for $LiMn_2O_4$ (0.16 eV[48]) might be attributed to such a regime. Apparently, small deviations (x) from stoichiometry ($Li_{1+x}Mn_2O_4$, $x > 0$ or $x < 0$, depending on preparation conditions) lead to drastic changes in the structure[45] and the electronic properties. The electrochemically active e_g electron when added to Mn^{IV} will tend to reside as close as possible to the intercalated Li atoms (see below) and provided the energy barrier of electron transfer is sufficiently small it will easily move along with Li^+ through the lattice. This is of great importance for the dynamics of Li.

IV. Conclusions

(1) DFT calculations on the Mn_7O_{14} and on MnO_6^{8-} cluster, embedded in a Madelung field of $6Mn^{4+}$ and $8O^{2-}$ ions, taken as point charges, enables us to characterize the Mn−O bonding as predominantly ionic. On the basis of the DFT calculations, a model is proposed to estimate electronic hopping, Mn−Mn and O−Mn charge-transfer parameters, and to calculate total energy diagrams while taking at the same time translational symmetry into account. The rather large energies for CT excitations, and the smaller integrals for d−d hopping, strongly suggest that a localized rather than a band model is a better approximation for the electronic structure as well as for the rather complex electronic and ionic transport properties.

(2) DFT calculations of the $Mn_7O_{14}^-$ cluster with a supplementary electron in the $2e_g$ orbital of Mn^{III} yield a large ground-state stabilization energy (−0.445 eV). This is due to displacements along the α_{1g} and the JT active ϵ_g modes, accompanied by a lengthening of the Mn−O bond and tetragonally elongated octahedra [$t_{2g}^3e_g(d_{z^2})^1$ ground state for Mn^{III}]. However, the mixing of these modes, which have the same symmetry in the C_s $Mn_7O_{14}^-$ cluster point group, reduces the vibronic coupling as compared to a MnO_6 cluster with distinct contributions from the α_{1g} and from the JT active ϵ_g modes. Such a coupling, which is frequently neglected when modeling the JT distortion in solids, may change sign and thus, become responsible for a vibronic enhancement (cooperative Jahn−Teller effect).

(3) A model of a small polaron is used to describe the electronic transport behavior in stoichiometric $LiMn_2O_4$ on the basis of vibronic coupling and electronic hopping energies, deduced from DFT cluster calculations. In the case of $Li_xMn_2O_4$ with $x < 1$ and with energetically equivalent d_{z^2} and $d_{x^2-y^2}$ orbitals the model provides the interesting hypothesis for an electronic transfer with a very low activation energy.

(4) The interaction of Li^+ with the electrochemically active electron (Li^+-e^-) leads to an effective screening of Li^+ from the large variation of the Madelung potential. As shown by a recent calculation using effective point charges,[49] the Madelung potential of Mn_2O_4 spinel favors the occupation of tetrahedral (8a) rather than octahedral (16c) sites by Li^+, and this is in agreement with the structure of $LiMn_2O_4$ in support of a predominantly ionic bonding of oxygen to $Mn^{III/IV}$ and Li^+. On the other hand, assuming that initially the extra electron resides on a Mn site [$2e_g(Mn^{III})$], the Li^+-e^- interaction is more attractive for the 16c site compared to the 8a site and this opposes the less favorable 8a → 16c change in the Madelung potential of Li^+. DFT calculations of the $LiMn_7O_{14}$ clusters with Li attached to a 8a and a 16c site yield indeed very close energies, implying that, within the cluster approximation, the two contribution nearly completely cancel with a slight preference of a 8a over 16c site occupancy.[50] A comparison between the energies of Li attached to Mn_7O_{14} clusters, with and without the Li^+-e^- interactions[49] indicates that this energy might be also effective in reducing the energy barrier of Li^+ when going from a tetrahedral 8a site to an octahedral 16c site (passing through the midpoint of a triangular O_3 plane shared between a O_4 tetrahedron and an O_6 octahedron). The Li−e interaction will be vanishingly small, however, if d electrons are delocalized forming band states, since their fraction on Mn and Li gets strongly reduced. One can conclude that localized d electrons, which is the case not only in Mn_2O_4 but in mixed-valent $Li_xMn_2O_4$ as well[51] would be a necessary condition for a fast diffusion of Li. On the other hand, the electron to which Li^+ is coupled has to have an energy barrier for electronic transfer which is accessible by thermal activation. The conditions for this have been specified in section III.3. In addition, partial transfer of this electron from $Mn^{III}(e_g)$ to Li^+ is expected to lower this barrier. As a result, diffusion of Li in $Li_xMn_2O_4$ seems to be a fast process, but actual diffusion coefficients of Li^+ in bulk $Li_xMn_2O_4$ and analogous materials remain to be explored by theoretical and experimental methods in future work.

Acknowledgment. This study was supported by the Swiss Federal Office of Energy. The authors owe thanks to Prof. Dr. R. Carr, Princeton, NJ, and to Prof. Dr. J. P. Malrieu, Toulouse, France, for useful discussions and to one anonymous reviewer for critical comments and suggestions.

Appendix

Deducing Metal−Metal Hopping Integrals from DFT Cluster Calculations. Here we describe a general procedure for calculating metal−metal hopping integrals from DFT results.

Let us denote the Kohn−Sham orbitals (resulting from a DFT calculation on a M_nL_m cluster; M, metals; L, ligands) which correspond to MO's dominated by *n*d orbitals with column vectors $\mathbf{C}_i$ and the corresponding eigenvalues with λ_i. From the components of the eigenvector matrix **V** build up from such columns one takes only the components corresponding to *n*d functions. Let us denote the matrix composed of the new column vectors by U and the diagonal eigenvalues matrix by $\mathbf{\Lambda}$ and introduce the overlap matrix S (eq A.1). Following the general

(48) Shimakawa, Y.; Numata, T.; Tabuchi, J. *J. Solid State Chem.* **1997**, *131*, 138.

(49) Atanasov, M.; Daul, C.; Barras, J.-L.; Benco, L.; Deiss, E. *Solid State Ionics* **1999**, *121*, 165.

(50) The situation changes when increasing the content of Li. Total energies for D_{3d} optimized $Li_6Mn_7O_{14}$ clusters show the preference of Li to occupy 16c rather then 8a cluster positions (16c, −161.3991 eV; vs 8a, −159.5244 eV), minimizing in this way unfavorable Li^+-Li^+ repulsive interactions. This is supported by structural results: while mixed 8a/16c occupancy with Li has been reported for the $Li_xMn_2O_4$ tetragonal spinel ($x > 1$), see: Thackeray, M. M.; David, W. I. F.; Bruce, P. G.; Goodenough, J. B. *Mater. Res. Bull.* **1983**, *18*, 461, the ordering of Li and Mn into layers of octahedral sites has been discovered in $Li_2Mn_2O_4$ (orthorhombic $LiMnO_2$, Hoppe, R.; Brachtel, G.; Jansen, M. *Z. Anorg. Allg. Chem.* **1975**, *417*, 1).

(51) Energies of $Mn^{IV}-e^-$ and Li^+-e^- interactions are calculated using the following DFT energies: $Li \rightarrow Li^+ + 1e^-$ ($\Delta E_1 = 5.35$ eV); $Li^+ + Mn_7O_{14} \rightarrow LiMn_7O_{14}^+$ ($\Delta E_2 = -1.18$ eV), $Mn_7O_{14} + 1e^- \rightarrow Mn_7O_{14}^-$ ($\Delta E_3 = -2.68$ eV) and $Li + Mn_7O_{14} \rightarrow LiMn_7O_{14}$ ($\Delta E_4 = -1.67$ eV), all DFT calculations for lithiated Mn_7O_{14} clusters being performed with one attached Li (8a) atom. From these data the effective (Li^+-e^-) coupling energy is given by $\Delta E_4 - \Delta E_1 - \Delta E_2 - \Delta E_3$. The $Mn^{IV}-e^-$ and Li^+-e^- energies (−2.68 and −3.16 eV, respectively) are comparable in magnitude and exceed the kinetic energy which is gained if d electrons delocalize on $t_{2g}(3d)$ and $e_g(3d)$ bands [cf. with −1.74 eV (t_{2g}) and − 0.3 eV (e_g) = ($^1/_2$) the bandwidths, as deduced from Mn−Mn hopping integrals]. It follows that electrons in lithiated Mn_2O_4 are localized on $Mn^{III}(e_g)$, but they are transfered partly from Mn^{III} to Li^+ via the bridging O atoms. A similar result deduced from band calculations on $LiCoO_2$ show indeed that upon delithiation electronic density is transferred back to Co(cf. refs 10 and 15).

theory of effective Hamiltonians,[52] one can calculate an effective Hamiltonian matrix $\mathbf{H}_{\text{Bloch}}$ on the bases of the *n*d orbitals of order $(5n) \times (5n)$ as given by eq A.2.[53] It should be noted that the matrix $\mathbf{H}_{\text{Bloch}}$ is in general not a

$$\mathbf{S} = \mathbf{U}\mathbf{U}^{\mathrm{T}} \tag{A.1}$$

$$\mathbf{H}_{\text{Bloch}} = \mathbf{U}\mathbf{\Lambda}\mathbf{U}^{\mathrm{T}}\mathbf{S}^{-1} \tag{A.2}$$

symmetric one. A symmetric matrix $\mathbf{H}_{\text{Bloch}}{}^{\mathrm{S}}$ can constructed though, taking the average of $\mathbf{H}_{\text{Bloch}}{}^{\mathrm{S}}$ and its transpose, $(\mathbf{H}_{\text{Bloch}})^{\mathrm{T}}$ (eq A.3). One alternative way in constructing a symmetric effective Hamiltonian $\mathbf{H}_{\text{desCloizeaux}}$ is given by (eq A.4).[54] Note that $\mathbf{U''U''}^{\mathrm{T}}$ ($\mathbf{U''} = \mathbf{S}^{-1/2}\mathbf{U}$) is a unit matrix.

$$\mathbf{H}_{\text{Bloch}}{}^{\mathrm{S}} = (^1/_2)(\mathbf{H}_{\text{Bloch}} + \mathbf{H}_{\text{Bloch}}{}^{\mathrm{T}}) \tag{A.3}$$

$$\mathbf{H}_{\text{desCloizeaux}} = \mathbf{S}^{-1/2}\mathbf{U}\mathbf{\Lambda}\mathbf{U}^{\mathrm{T}}\mathbf{S}^{-1/2} = \mathbf{S}^{-1/2}\,\mathbf{H}_{\text{Bloch}}\,\mathbf{S}^{1/2} \tag{A.4}$$

Calculations show that for the system under consideration recipes A.2 and A.3 and A.4 give numerically very close results.

(52) Durand, Ph.; Malrieu, J. P. *Advances in Chemical Physics*; Wiley: New York, 1987; Vol. 67 and references therein.

(53) Bloch, C. *Nucl. Phys.* **1958**, *6*, 329; one can easily find $\mathbf{S}^n$ ($n = -1, -^1/_2$) using the following recipe; (i) diagonalize **S** and get eigenvalues $\mathbf{\Lambda}_{\mathrm{S}}$ (diagonal) and eigenvector (in columns) U_{S} matrices. (ii) $\mathbf{S}^n$ is then given by $\mathbf{U}_{\mathrm{S}}{}^{\mathrm{T}}\mathbf{\Lambda}_{\mathrm{S}}{}^n\mathbf{U}_{\mathrm{S}}$.

(54) des Cloizeaux, *Nucl. Phys.* **1960**, *20*, 321.

If we denote $\mathbf{H}_{\text{Bloch}}{}^{\mathrm{S}}$ or $\mathbf{H}_{\text{desCloizeaux}}$ by **H**, metal−metal hopping integrals are calculated as follows: one diagonalizes **H**, omitting matrix elements between d-orbitals located on different centers. Let **U′** be matrix composed of the resulting eigenvectors. The effective coupling matrix $\mathbf{H}_{\text{eff}}$ is then given by eq A.5. $\mathbf{H}_{\text{eff}}$ has the property of

$$\mathbf{H}_{\text{eff}} = \mathbf{U'}^{-1}\,\mathbf{H}\mathbf{U'} = \mathbf{U'}^{\mathrm{T}}\mathbf{H}\mathbf{U'} \tag{A.5}$$

being block-diagonal for *n*d orbitals belonging to the same metal center. The diagonal elements correspond to eigenfunctions of the ligand-field operator, an the eigenvectors to the ligand field orbitals on each center. The 5×5 block matrices (in general off-diagonal) connecting *n*d orbitals located on different metal centers are the corresponding M−M hopping integrals.[55] Another procedure in calculating such integrals within the angular overlap model has been described elsewhere.[26] The fit of the AOM expressions to the hopping integrals obtained from the DFT data yields the relative contributions of direct and indirect (via bridging ligands) metal−metal coupling. Such matrix elements can be used in Hubbard models (cf. section III.1.2.1) or they can be applied to treat magnetic exchange coupling in dimers and extended structures of transition metal ions.[28]

JA9904484

(55) For a similar procedure, see: Lee, S. *J. Am. Chem. Soc*. **1989**, *111*, 7754.